

# A performance evaluation method based on the Pareto frontier for enhanced microchannel heat sinks

Min Yang<sup>a,b</sup>, Mo-Tong Li<sup>b</sup>, Xin-Gang Yu<sup>a</sup>, Lei Huang<sup>a</sup>, Hong-Yang Zheng<sup>a</sup>, Jian-Yin Miao<sup>a</sup>, Bing-Yang Cao<sup>b,\*</sup>

<sup>a</sup> Beijing Key Laboratory of Space Thermal Control Technology, Beijing Institute of Spacecraft System Engineering, China Academy of Space Technology, Beijing 100094, PR China

<sup>b</sup> Key Laboratory for Thermal Science and Power Engineering of Ministry of Education, Department of Engineering Mechanics, Tsinghua University, Beijing 100084, PR China

## ARTICLE INFO

### Keywords:

Enhanced microchannel heat sinks  
Thermal and hydraulic performance  
Performance evaluation  
Pareto frontier  
Design Optimization Area

## ABSTRACT

A performance evaluation method based on the Pareto frontier for different types of enhanced microchannel heat sinks has been proposed and applied to find the best comprehensive performance. The concept of Design Optimization Area (DOA) developed in our previous work is used for comprehensive evaluation and a microchannel heat sink within DOA means that the pumping power  $P_p$  and the total thermal resistance  $R_t$  could be both reduced compared with user demands. The comprehensive evaluation method consists of three steps: (1) conducting a multi-objective optimization of various microchannel structures to obtain the Pareto frontiers; (2) determining DOA above those Pareto frontiers based on user demands; (3) selecting the best one with the largest DOA. The immediacy and practicability of the method are verified through comparative studies. Detailed comparisons through this method between a hybrid microchannel heat sink and other three enhanced microchannel structures have been conducted. The results indicate that the hybrid microchannel has superior performance and it enables a lower  $P_p$  under the same  $R_t$ . The proposed evaluation method can also be applied to evaluate the comprehensive performance of various heat exchangers by changing the optimization objectives according to the limits or priorities of users.

## 1. Introduction

With the ever-increasing of processing performance and die packaging density, the incorporated transistors in electronics and the corresponding power density have risen sharply [1–3]. Consequently, thermal management has become one of the essential challenges for the future of various electronic devices and efficient cooling solutions are needed to satisfy their cooling demands [4–8]. In 1981, the concept of microchannel heat sink was proposed [9] and has drawn more and more attention due to its high heat extraction capability and high reliability [10–12]. However, traditional microchannel heat sink with straight, parallel microchannels suffers from two drawbacks [13]. On the one hand, the continuous growth of thermal boundary layer along the microchannel will bring a large nonuniform temperature distribution across the chip, which can result in thermal stress. In addition, a large pumping-power consumption is also needed due to the exorbitant pressure drop across the microchannel heat sink. Various passive

strategies by optimizing channel structure have been developed and studied to improve the thermal and hydraulic performance of the traditional microchannel heat sink. Generally speaking, those microchannel structures can be divided into three broad categories and Table 1 summarizes some typical structures of these three types of microchannels:

- (1) The continuous microchannel: this microchannel type has continuous fin cross section and can enhance the flow disturbance and thin boundary layer by utilizing special channel shapes, such as microchannel mounted with triangular ribs [14], wavy microchannel [15], microchannel with structured wall surface roughness [16], or placing vortex generators in the microchannel, such as herringbone-inspired microstructures [17], wire coil inserts [18], etc. The pressure drop penalty is a limiting factor for this type of enhanced microchannel structure.

\* Corresponding author.

E-mail address: [caoby@tsinghua.edu.cn](mailto:caoby@tsinghua.edu.cn) (B.-Y. Cao).

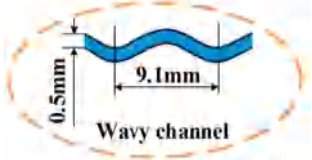
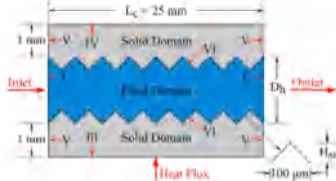
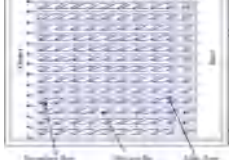
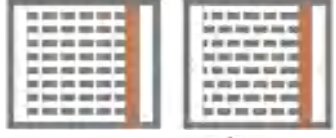
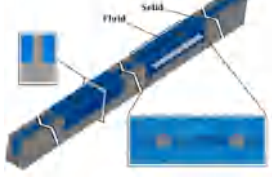
<https://doi.org/10.1016/j.applthermaleng.2022.118550>

Received 30 August 2021; Received in revised form 15 March 2022; Accepted 19 April 2022

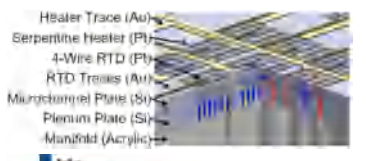
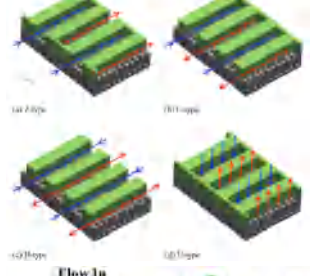
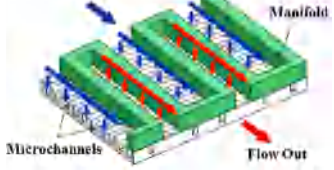
Available online 22 April 2022

1359-4311/© 2022 Elsevier Ltd. All rights reserved.

**Table 1**  
Summary of some typical structures of three types of microchannel structures.

Authors	Types	Structures of microchannel
Chai et al. (2019) [14]	Continuous (triangular ribs on sidewalls)	
Chen et al. (2021) [15]	Continuous (wavy channel)	
Singh et al. (2021) [16]	Continuous (structured wall surface roughness)	
Marschewski et al. (2016) [17]	Continuous (herringbone-inspired microstructures)	
Feng et al. (2017) [18]	Continuous (wire coil inserts)	
Xu et al. (2008) [19]	Interrupted	
Lee et al. (2009) [20]	Interrupted (oblique fins)	
Huang et al. (2017) [21]	Interrupted (slotted microchannel)	
Feng et al. (2021) [22]	Interrupted (microchamber and circular pin-fin)	
Gao et al. (2021) [23]	Interrupted (trapezoidal fins)	
Drummond et al.	Manifold (a hierarchical)	

**Table 1 (continued)**

Authors	Types	Structures of microchannel
(2019) [24]	manifold distributor)	
Li et al. (2019) [25]	Manifold	
Luo et al. (2020) [26]	Manifold (Z/C/H/U-types)	
Yang et al. (2020) [27]	Manifold (secondary channels)	
van et al. (2021) [28]	Manifold	

- (2) The interrupted microchannel: this microchannel type has interrupted fins by slotting the microchannel wall. It can also bring enhanced fluid mixing and thinner boundary layer thickness by secondary flow and vortex [19–23]. Similarly, the interrupted flow path always brings an extra pumping-power consumption.
- (3) The manifold microchannel: this microchannel type consists of a channel component that has alternating inlets and outlets used for coolant distribution, which can greatly reduce the pumping-power consumption due to a considerable flow length reduction in microchannel [24–28]. In addition, a better thermal performance can be observed when using the manifold structure due to the jet-impingement.

For those existing and upcoming types of microchannel heat sinks, it is a challenge to find the best one. Considering that a microchannel heat sink with superior comprehensive performance should enable a reasonable temperature of the electronic devices with the lowest pumping-power consumption, the total thermal resistance  $R_t$  and pumping power  $P_p$  are two essential evaluation criteria that many researchers have adopted to evaluate their microchannel heat sinks. Here, the thermal resistance  $R_t$  is defined as:

$$R_t = \frac{\Delta T_{\max}}{Q} = \frac{T_{\max} - T_{\text{in}}}{Q} \quad (1)$$

where  $T_{\max}$  and  $T_{\text{in}}$  are the maximum temperature of the microchannel heat sink base and the fluid temperature at the inlet,

respectively.  $Q$  is the total heat flux applied to the backside of the heat sink and is defined as  $Q = q'' \times A_{hs}$ , where  $A_{hs}$  is the area of the heat source, i.e. the area of the microchannel heat sink backside. And the pumping power  $P_p$  is calculated as:

$$P_p = \Delta P \cdot \dot{V} \quad (2)$$

where  $\Delta P$  is the pressure drop between inlet and outlet while  $\dot{V}$  is the volumetric flow rate. Nevertheless, it's hard to compare  $R_t$  under the same  $P_p$  because in practice,  $\Delta P$  and  $\dot{V}$  cannot be determined simultaneously and it's impossible to keep  $P_p$  the same either in experiment or in simulation. Therefore, an accurate and rapid method combining the hydraulic with thermal performance for comprehensive assessment of various microchannel heat sinks is needed. Some beneficial attempts have been carried out to find out a more reasonable evaluation criteria or method for various heat transfer enhancement structures [29–33]. However, as demonstrated in our previous study [34], as for microchannel heat sink, no positive correlation can be established between the convective heat transfer area and thermal performance, which means that larger convective heat transfer area would not necessarily bring smaller maximum chip temperature, smaller total thermal resistance, or larger average heat transfer coefficient. The thermal performance is influenced by many geometrical parameters, rather than becoming better with the convective heat transfer area increasing. In addition, as for microchannel heat sink obtained by micro/nano fabrication technology, there's no need to take into account the value of the convective heat transfer area because it has nothing to do with the cost. Therefore, those existing multiple evaluation criteria related to the convective heat transfer area, such as  $h$ ,  $Nu$ ,  $PEC$  etc., may be not very reasonable for evaluating the thermal performance of different microchannel structures. Furthermore, the existing methods always evaluate the heat sinks with given geometric parameters based on the selected thermal and flow parameters. However, it's necessary to select the optimal designs of different types of microchannel structures rather than arbitrary ones when comparing their performance. As a result, it is needed to consider both  $R_t$  and  $P_p$  as the optimization objectives and compare the optimal designs to decide which type of microchannel structures is superior. Since the two objectives are almost in conflict with each other, the multi-objective optimization indicates that there is no single optimal solution, but rather a set of solutions composed of multiple or even infinite Pareto-optimal solutions [35]. Therefore, comparing the Pareto-optimal solutions of different heat sinks is a more reasonable approach for evaluating the comprehensive performance of different microchannel structures. In this study, an accurate and rapid method for comprehensive evaluation of different microchannel heat sinks has been proposed. The method selects the best one from multiple microchannel heat sinks through comparing the Pareto-optimal solutions of different enhanced structures. Those sample points required by the multi-objective optimization can be obtained automatically by integrating various operations (such as model constructing, mesh generating and computational fluid dynamics calculating) together through a software platform. It should be noted that this method can be also applied to various heat exchangers by changing the optimization objectives based on the limits or priorities of users.

## 2. Construction of the performance evaluation method

This section introduces the specific steps and features of the comprehensive evaluation for different types of microchannel heat sinks, including an example to show the DOA determination method. Moreover, careful comparisons are made to illustrate the immediacy and accuracy of the comprehensive evaluation method. It should be pointed out that those Pareto frontiers used in the following analyses in this section are not real but are created to present the characteristics of the performance evaluation method.

### 2.1. Evaluation method procedures

The Evaluation method procedure steps are as follows:

(1) Conduct a multi-objective thermal and hydraulic design optimization of various microchannel heat sinks to obtain the Pareto frontiers. Minimizing the pumping-power consumption  $P_p$  and thermal resistance  $R_t$  at the same time is the optimization objective. Obviously, the trade-off between  $R_t$  and  $P_p$  will be established, since these two objectives are in conflict with each other, which means that as  $P_p$  decreases,  $R_t$  will increase. Therefore, a set of solutions, namely Pareto-optimal solutions will be obtained. Every solution of the Pareto-optimal solutions is the best trade-off between the total thermal resistance and pumping power. A concave curve named Pareto frontier will be formed and it represents the performance limitation. In addition, Pareto frontiers of different enhanced microchannel structures can be obtained with high efficiency through the novel optimization approach developed in our previous work [35];

(2) Determine the region of Design Optimization Area (DOA) above those Pareto frontiers based on the limits or priorities of users. As described in our previous work [34], each datum point within the DOA represents the pumping power and the thermal resistance can be both reduced. Consequently, the DOA size can be used to characterize the comprehensive performance of a given type of microchannel heat sink, and a larger DOA means that more microchannel heat sinks of this type with specific geometric parameters can satisfy user demands. Method for DOA determination will be described below;

(3) Select the best enhanced microchannel structure with the largest DOA area. As for a specific heat dissipation problem in practice, the design optimization should be conducted under the same design constraints required by users, such as the design space (e.g. the cooling area, the size of the substrate used for obtaining enhanced microchannels), thermal conditions (e.g. the heating power, the thermal boundary), heat sink material, coolant, acceptable maximum temperature and temperature uniformity and available pumping power. Besides, the users can determine which types of microchannels (as we mentioned above) can be selected and decide what parameters of these structures can be set as the variables. After that, the multi-objective optimization can be carried out to obtain the Pareto frontiers and compare the DOAs of different types.

### 2.2. DOA determination method

As shown in Fig. 1, assuming that those Pareto-optimal solutions (i.e. Pareto frontier) of a given microchannel heat sink (continuous

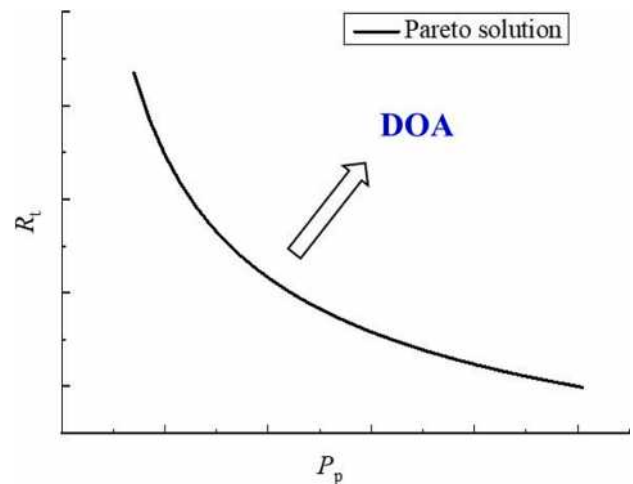


Fig. 1. Definition of DOA for a given Pareto frontier without requirements on pumping power  $P_p$  and thermal resistance  $R_t$ .

microchannel, interrupted microchannel or manifold microchannel) are obtained through a multi-objective optimization. The determination process for DOA is based on the requirements of users. Generally, those requirements can be divided into four broad categories according to users:

- (1) Without requirements, because of the Pareto frontier indicating the performance limitation of a corresponding heat sink, the region above the Pareto frontier is defined as DOA if the users accept arbitrary pumping-power consumption  $P_p$  and thermal resistance  $R_t$ . A reduction in  $P_p$  and  $R_t$  can be observed simultaneously for data points within DOA;
- (2)  $P_p$  requirement, if  $P_p < P_{p1}$  is required by users, DOA is defined as the region enclosed by the line  $P_p = P_{p1}$  and the Pareto frontier, as shown in Fig. 2;
- (3)  $R_t$  requirement, if  $R_t < R_{t1}$  is required by users, DOA is defined as the region enclosed by the line  $R_t = R_{t1}$  and the Pareto frontier, as shown in Fig. 3;
- (4)  $P_p$  and  $R_t$  requirements, if  $P_p < P_{p1}$  and  $R_t < R_{t1}$  are both required by users, similarly, DOA is defined as the region enclosed by the line  $P_p = P_{p1}$ , the line  $R_t = R_{t1}$  and the Pareto frontier together, as shown in Fig. 4. Actually, to ensure the safety and longevity of the driven pump and electronics, some specific operating conditions may be required by users. For example, there are only three operating conditions can be accepted by users and we can select the one that can satisfy users cooling demands through the relative position between those operating conditions and the Pareto frontier.

The above determination process for DOA is based on a single type of heat sink under different user demands. Next, the practicability and visualization of the comprehensive evaluation method will be verified through careful comparisons between the Pareto frontiers of two types of heat sinks, namely type-I and type-II. Generally, within the range under discussion, the two Pareto frontiers may intersect or separate each other under the same operating conditions.

(1) Specific operating condition requirements

Case 1. Disjoint Pareto frontiers.

As shown in Fig. 5, there are only three operating conditions can be accepted by users and we define those as 1#, 2# and 3# from bottom to top. As for 1# operating condition, neither type-I heat sink nor type-II heat sink can satisfy the cooling demands. It is necessary to develop new types of heat sinks with better overall performance. As for 2#

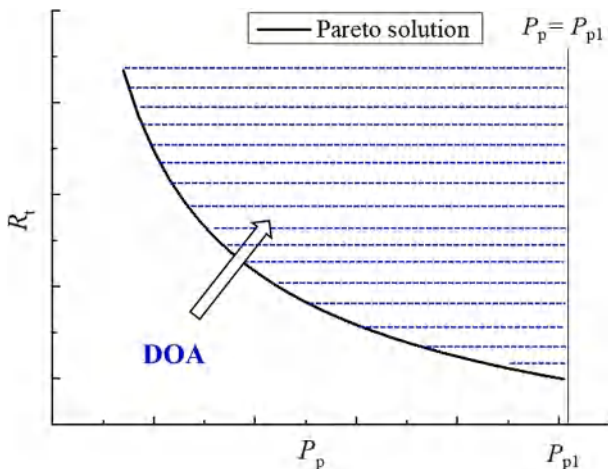


Fig. 2. Definition of DOA for a given Pareto frontier with requirement on pumping power  $P_p$ .

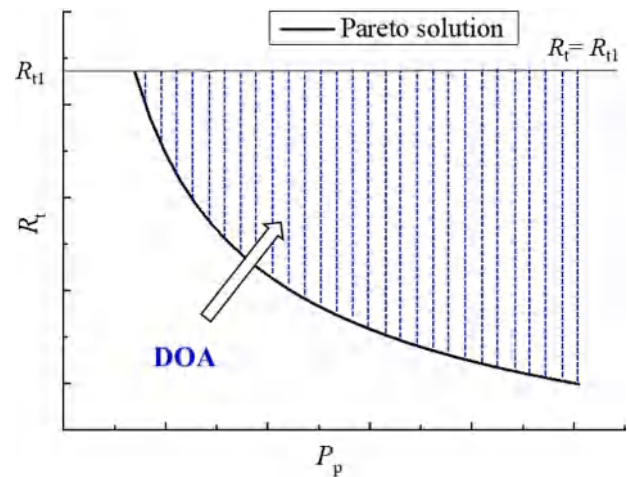


Fig. 3. Definition of DOA for a given Pareto frontier with requirement on thermal resistance  $R_t$ .

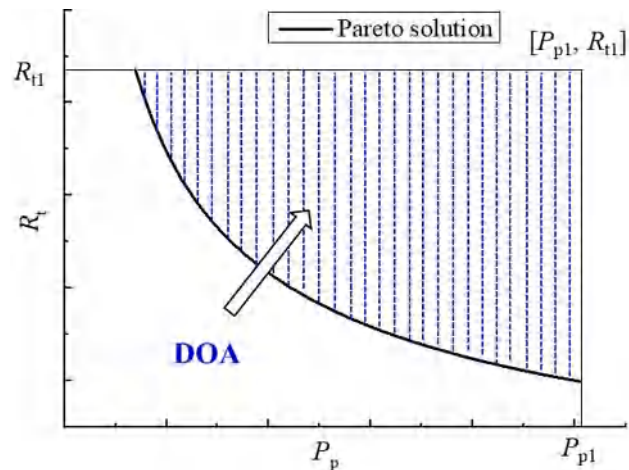


Fig. 4. Definition of DOA for a given Pareto frontier with requirements on pumping power  $P_p$  and thermal resistance  $R_t$ .

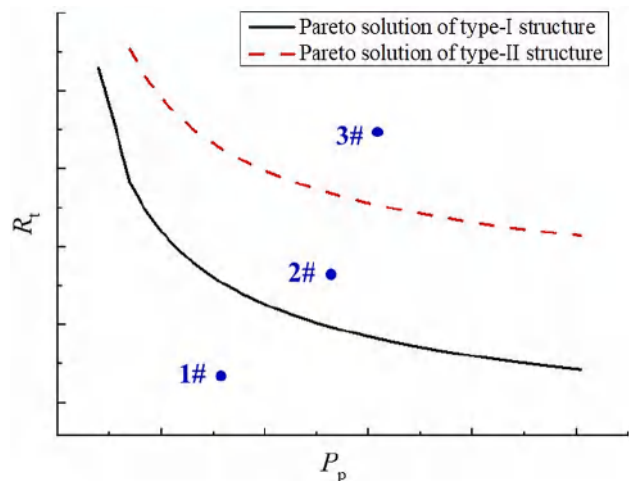


Fig. 5. Two disjoint Pareto frontiers of type-I and type-II heat sinks and three operating conditions required by users.

operating condition, it is type-I heat sink, but not type-II heat sink, that can meet the user demands. Similarly, as for 3# operating condition, both type-I heat sink and type-II heat sink can satisfy the cooling demands.

Case 2. Intersected Pareto frontiers.

As shown in Fig. 6, it is easy to understand that new types of heat sinks with better overall performance should be proposed under 1# operating condition. Type-I heat sink can satisfy the cooling demands under 2# or 4# operating condition and type-II heat sink can satisfy the cooling demands under 3# or 4# operating condition.

(2)  $P_p$  requirement, i.e.  $P_p < P_{p1}$

Case 1. Disjoint Pareto frontiers.

As mentioned above, if  $P_p < P_{p1}$  is required by users, DOA is defined as the region enclosed by the line  $P_p = P_{p1}$  and the Pareto frontier. Fig. 7 shows a clear comparison between the DOA of type-I heat sink and that of type-II heat sink. Type-I heat sink has larger DOA, which means that more microchannel heat sinks of this type with specific geometric parameters can satisfy user demands. The shadow region in Fig. 7 indicates the larger DOA of type-I compared with that of type-II.

Case 2. Intersected Pareto frontiers.

As shown in Fig. 8, a distinction is made between the DOA comparison and it can be divided into two parts based on the intersection, which is defined as  $(P_{p0}, R_{t0})$ . Here, we take the line  $P_p = P_{p0}$  as the dividing line to explain the DOA analysis. Clearly, it can be seen that type-II heat sink has larger DOA on the left of the line  $P_p = P_{p0}$ . By contrast, type-I heat sink has larger DOA on the right of the line  $P_p = P_{p0}$ .

(3)  $R_t$  requirement, i.e.  $R_t < R_{t1}$

Case 1. Disjoint Pareto frontiers.

As mentioned above, if  $R_t < R_{t1}$  is required by users, DOA is defined as the region enclosed by the line  $R_t = R_{t1}$  and the Pareto frontier. As can be seen from Fig. 9, it is obvious that type-I heat sink has larger DOA, which means that more microchannel heat sinks of this type with specific geometric parameters can satisfy user demands. The shadow region in Fig. 9 illustrates the larger DOA of type-I compared with that of type-II.

Case 2. Intersected Pareto frontiers.

Here, the line  $R_t = R_{t0}$  is selected as the dividing line to explain the DOA analysis. Fig. 10 shows a clear comparison between the DOA of type-I heat sink and that of type-II heat sink. It is obvious that Type-I heat sink has larger DOA than Type-II below the line  $R_t = R_{t0}$ . By contrast, Type-II heat sink has larger DOA than Type-I above the line  $R_t$

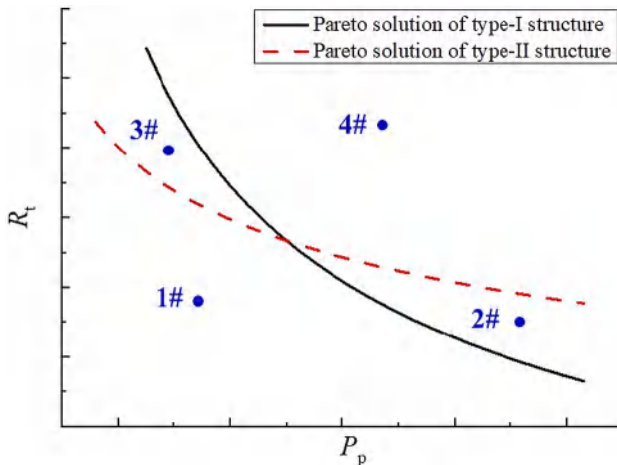


Fig. 6. Two intersected Pareto frontiers of type-I and type-II heat sinks and four operating conditions required by users.

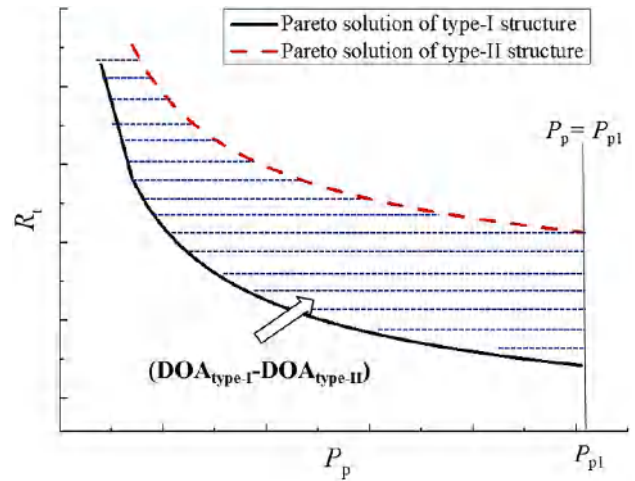


Fig. 7. Comparison of DOA for two disjoint Pareto frontiers of type-I and type-II heat sinks.

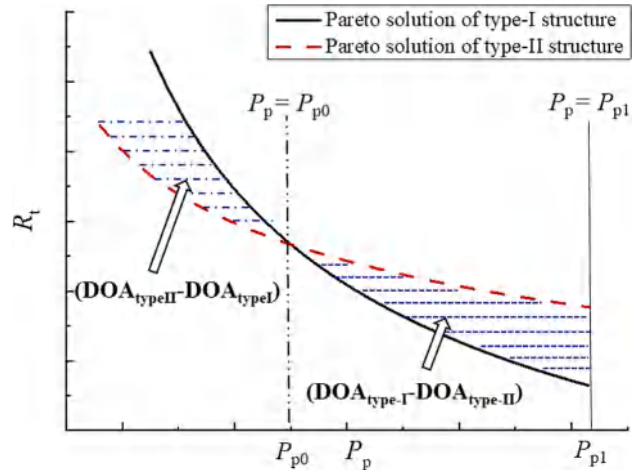


Fig. 8. Comparison of DOA for two intersected Pareto frontiers and it can be divided into two parts according to the line  $P_p = P_{p0}$ .

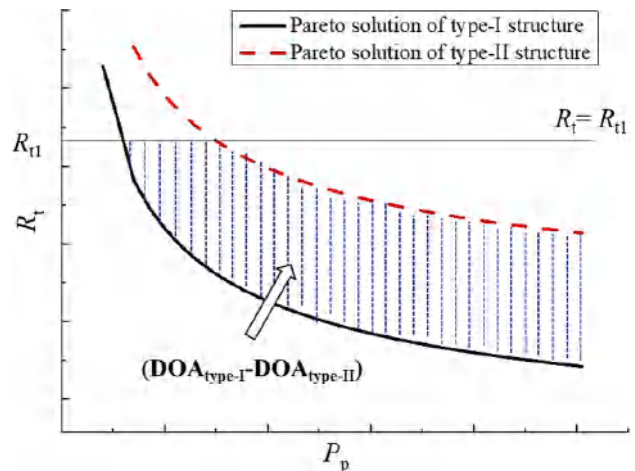


Fig. 9. Comparison of DOA for two disjoint Pareto frontiers of type-I and type-II heat sinks.

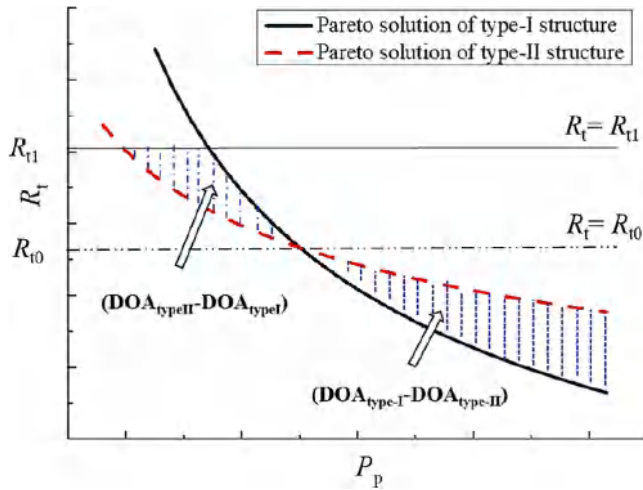


Fig. 10. Comparison of DOA for two intersected Pareto frontiers and it can be divided into two parts according to the line  $R_t = R_{t0}$ .

=  $R_{t0}$ .

(4)  $P_p$  and  $R_t$  requirements, i.e.  $P_p < P_{p1}$  and  $R_t < R_{t1}$

Case 1. Disjoint Pareto frontiers.

As mentioned above, if  $P_p < P_{p1}$  and  $R_t < R_{t1}$  are both required by users, similarly, DOA is defined as the region enclosed by the line  $P_p = P_{p1}$ , the line  $R_t = R_{t1}$  and the Pareto frontier together. As shown in Fig. 11, it is obvious that type-I heat sink has larger DOA than type-II heat sink. There are more microchannel heat sinks of type-I with specific geometric parameters that can meet the thermal and hydraulic performance demands.

Case 2. Intersected Pareto frontiers.

The line  $P_p = P_{p0}$  is taken as the dividing line. As shown in Fig. 12, type-II heat sink has larger DOA than that of type-I heat sink on the left of line  $P_p = P_{p0}$ . By contrast, type-I heat sink has larger DOA than that of type-II heat sink on the right of line  $R_t = R_{t0}$ .

Certainly, the proposed performance evaluation method may encounter the situation that those Pareto frontiers of different types of enhanced microchannels are very close. Obviously, those types of enhanced microchannels have the almost same comprehensive performance and which one to choose depends on the limits or priorities of users. Moreover, it should be noted that the Pareto frontiers of different

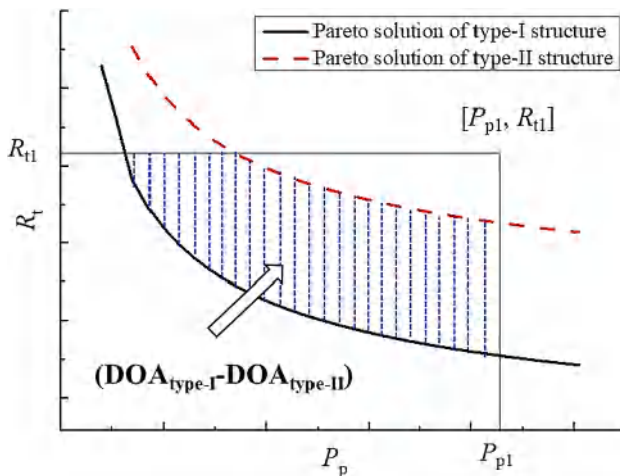


Fig. 11. Comparison of DOA for two disjoint Pareto frontiers of type-I and type-II heat sinks.

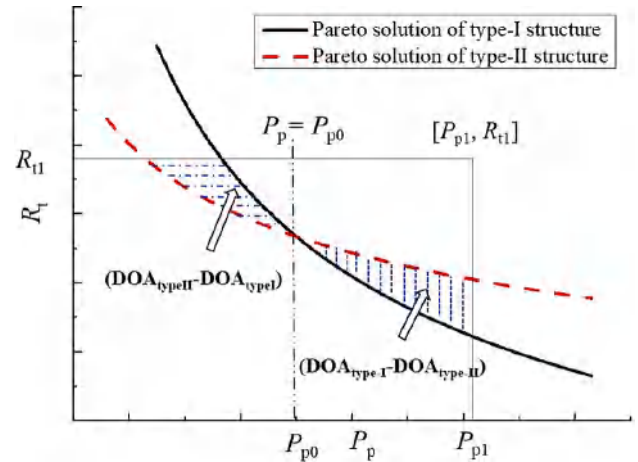


Fig. 12. Comparison of DOA for two intersected Pareto frontiers and it can be divided into two parts according to the line  $P_p = P_{p0}$ .

enhanced structures shown above are assumed to be obtained at the same operational conditions.

### 3. Validation and application of the performance evaluation method

In order to validate the immediacy and accuracy of the comprehensive performance evaluation method, comparative studies between the hybrid microchannel heat sink combining manifold distributor with secondary channels proposed in our previous study [34,35] and other three enhanced microchannel structures, namely microchannel heat sink with wire coil inserts [18], microchannel heat sink with cavity and rib [36] and interrupted microchannel heat sink with rib [37] are conducted. The heat sink we proposed before contains trapezoid fins in microchannel. The coolant is water and the substrate is silicon. And the multi-objective optimization was performed under uniform heat flux of  $200 \text{ W/cm}^2$  with four dimensionless design variables which are defined based on those geometric parameters shown in Fig. 13 (b). The optimization domain contains 10 channels and the channel length is  $10.6 \text{ mm}$ , which represents a completed heat sink.

Besides, we also compare the straight rectangle microchannel heat sink [38] and the microchannel heat sink with a grooved structure [39] to illustrate the application in intersected Pareto frontiers.

As shown in Fig. 14 (a), Feng et al. [18] designed four different kinds of microchannel heat sinks with wire coil inserts: microchannel with long wire coil at the center line (LWCC), microchannel with long wire coil on the bottom (LWCB), microchannel with three segments of short wire coil at the center line (SWCC) and microchannel with three segments of short wire coil on the bottom (SWCB). The additional wire coil can intensify the flow disturbance, thereby thinning the boundary layer and enhancing heat transfer. They carried out numerical simulation using water as coolant with uniform heat fluxes of  $20$  and  $40 \text{ W/cm}^2$  respectively. Here, they carried out the optimization with a computational domain of  $40 \text{ mm} \times 1.5 \text{ mm}$  and the solid domain was set as copper. As shown in Fig. 14 (b), those four enhanced microchannel heat sinks they designed have lower thermal resistance when comparing with that of the plain rectangular (PR) microchannel heat sink under the same pumping power. In addition, those four  $R_t$ - $P_p$  data points of LWCC, LWCB, SWCC and SWCB almost coincided under different heat fluxes, indicating that those data points may around the Pareto-optimal solutions. Therefore, data points with the lowest  $R_t$  under the same  $P_p$  are figured out and assumed as the Pareto frontier of the microchannel with wire coil inserts.

Fig. 15 illustrates a clear comparison between the two Pareto frontiers of the hybrid microchannel and the microchannel with wire coil

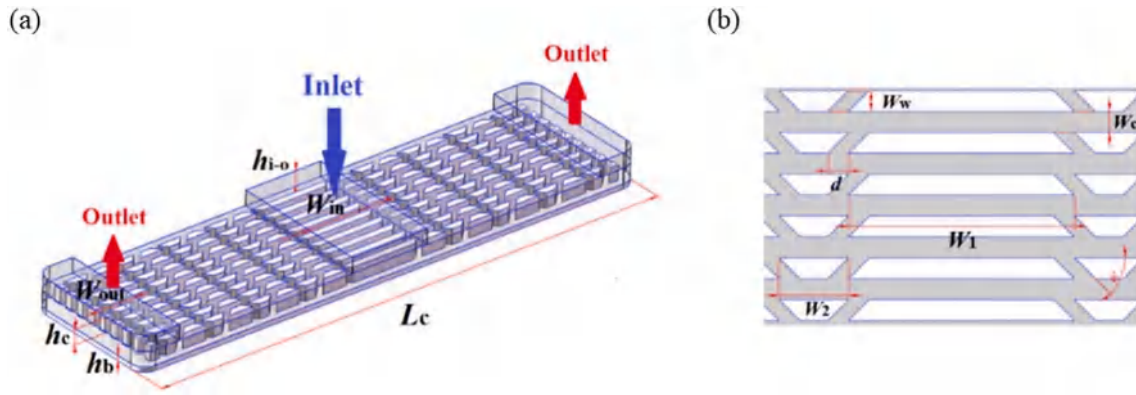


Fig. 13. (a) The schematic diagram of the hybrid microchannel heat sink and (b) the optimization geometric parameters in our previous work [35].

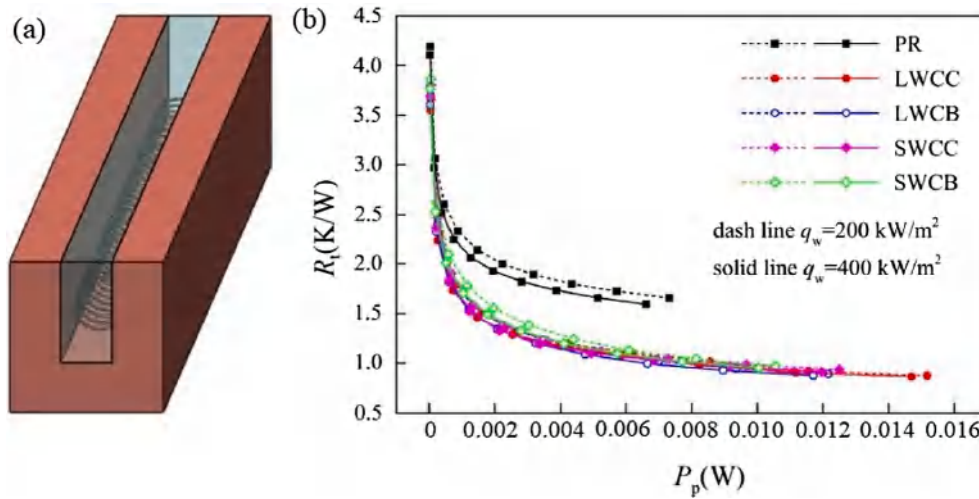


Fig. 14. (a) The structure of the rectangular microchannel heat sink with wire coil inserts and (b) numerical simulation results of Feng et al. [18].

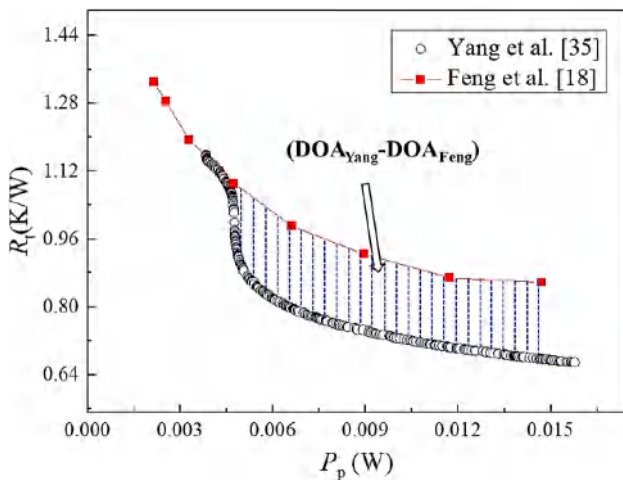


Fig. 15. Comparison of the DOA between the hybrid microchannel heat sink in our study [35] and the enhanced structure designed by Feng et al. [18].

inserts. As mentioned above, Feng et al. simulated the single microchannel which demands less pumping power and has better thermal performance than a completed heat sink. Besides, the channel material, copper, in their study has a thermal conductivity of 400 W/m-K approximately while silicon used in our design is 159 W/m-K. However, it is obvious that the hybrid microchannel heat sink proposed in our

previous work can maintain a lower  $R_t$  under the same  $P_p$  in most cases. The shadow region in Fig. 15 represents the larger DOA of our hybrid microchannel compared with that of Feng’s structure.

Zhai [36] presented another complex microchannel heat sinks by adding internal ribs into two cavities (Fig. 16 (a)). Vortices in the cavity zones are observed due to the sudden enlargement area and reduced velocity, which can help to strengthen the mixing of cold and hot coolant. A multi-objective thermal and hydraulic design optimization of the microchannel structure was conducted with deionized water as coolant at a given heat flux of 100 W/cm<sup>2</sup>. The optimization domain is 10 mm in length with single silicon-based channel. Those Pareto-optimal solutions are plotted in Fig. 16 (b). Similarly, Fig. 17 gives a clear comparison between the two Pareto frontiers of the hybrid microchannel and the microchannel with cavity and rib. It is obvious that our design can maintain a lower  $R_t$  under the same  $P_p$ . The shadow region describing the larger DOA of our hybrid microchannel compared with that of Zhai’s structure is also marked. Besides, the size of our computational domain is larger than that of Zhai’s, it means that our structure needs to dissipate more heat with longer total fluid path. Therefore, our design has a better comprehensive performance.

Fig. 18(a) shows the microchannel heat sink with ribs in the interrupted transverse developed by Chai et al. [37]. They studied interrupted microchannel heat sinks with five different rib configurations, i. e. rectangular (IMCHS-R), backward triangular (IMCHS-BT), diamond (IMCHS-D), forward triangular (IMCHS-FT) and ellipsoidal (IMCHS-E). The interrupted microchannel without ribs (IMCHS) was also selected. The numerical simulation was performed on a control volume

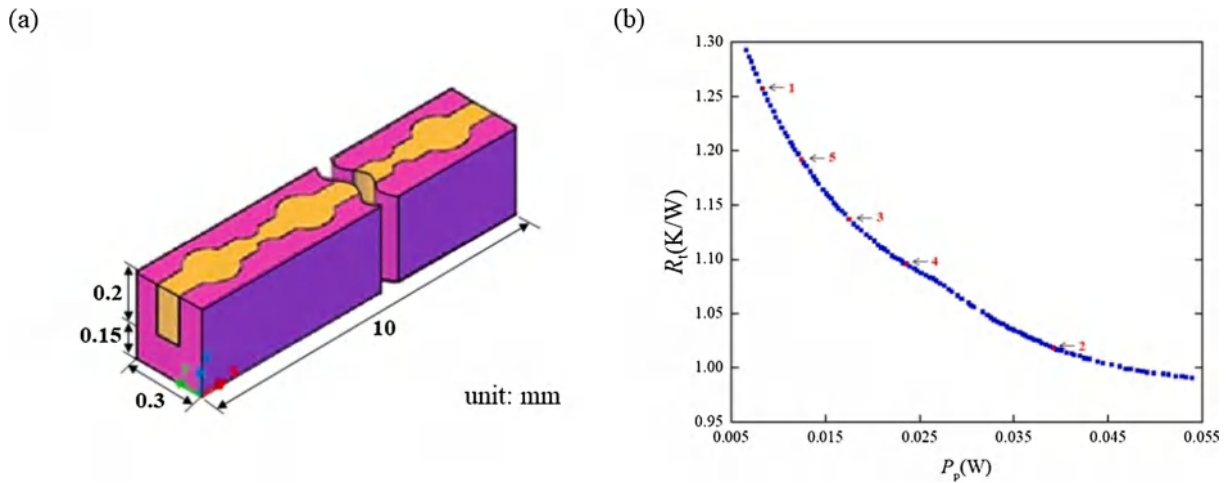


Fig. 16. (a) The microchannel structure with cavity and rib and (b) the Pareto frontier obtained from a multi-objective optimization (Zhai [36]).

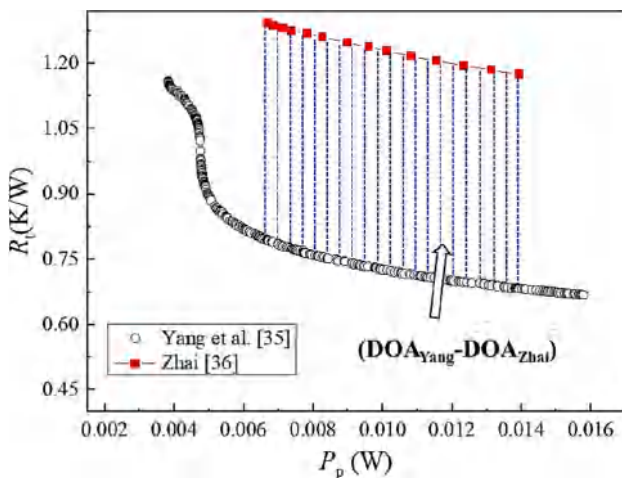


Fig. 17. Comparison of the DOA between the hybrid microchannel heat sink in our study [35] and the enhanced structure designed by Zhai [36].

containing a single microchannel and surrounding solid along with the silicon base at a heat flux of  $100 \text{ W/cm}^2$ . The coolant is water and the channel length is set as 10 mm. Compared with straight, parallel microchannels (MCHS), the special design can reduce the total thermal resistance and the total entropy generation rate by 4–31% and 4–26%, respectively, as shown in Fig. 18(b). Since Chai et al. specified the design

domain of the rib (0.5 mm in length) and the five  $R_t$ - $P_p$  curves of different ribs almost coincided, it indicates that those data points could be approximated as Pareto-optimal solutions.

Similarly, Fig. 19 shows the comparison between the two Pareto frontiers of the hybrid microchannel and the interrupted microchannel with rib. Due to the fact that our design selected a larger computational domain but maintain a lower  $R_t$  under the same  $P_p$ , it means that our design has a better overall performance. The shadow region describing the larger DOA of the hybrid microchannel compared with that of Chai's structure is also marked.

Ansari et al. [39] presented a grooved heat sink (Fig. 20 (c)) which enhanced the convective heat transfer due to the increase in heat exchange area and convective heat transfer coefficient compared with the same smooth microchannel in depth. They conducted multi-objective optimization and obtained the Pareto frontier as shown in Fig. 20 (d). Another study [38] focused on the geometric optimization of traditional rectangle microchannel heat sink (Fig. 20 (a)). They adopted the empirical correlation of the total thermal resistance and pumping power and use the augmented  $\epsilon$ -constraint method to get the Pareto frontier (Fig. 20 (b)). Both designs set the single microchannel region with 10 mm in length as the computational domain and optimized with water as coolant and silicon as heat sink material.

The comparison of the DOAs is illustrated in Fig. 21. It indicates that if  $P_p < 0.13 \text{ W}$ , the structure proposed by Ansari et al. [39] has a larger DOA and performs better in heat dissipation, while if  $P_p > 0.13 \text{ W}$ , it is better to select the rectangle microchannel in the work of Kwanda et al. [38], of which the DOA is larger. The left shadow region describes the larger DOA of the grooved structure in the study of Ansari et al. [39]

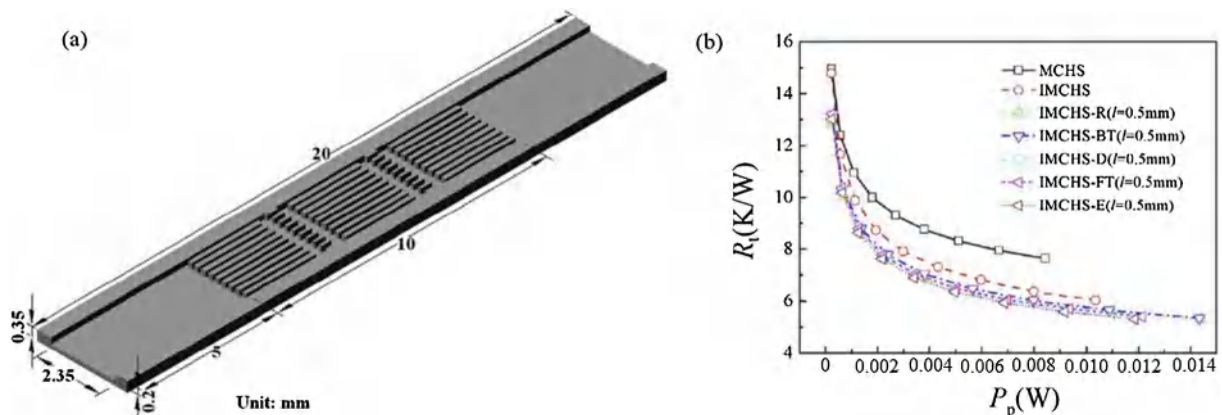


Fig. 18. (a) The structure of the microchannel heat sink and (b) numerical simulation results of Chai et al. [37].

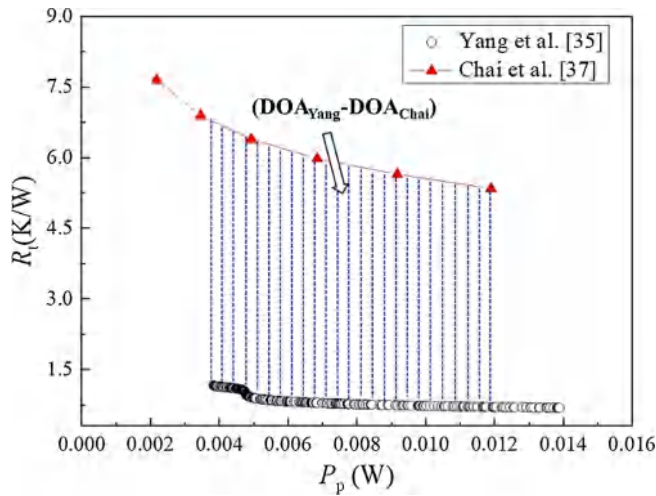


Fig. 19. Comparison of DOA of the microchannel heat sink in our study [35] and that proposed by Chai et al. [37].

compared with the rectangle microchannel and the right shadow region describes the larger DOA of the rectangle microchannel in the study of Kwanda et al. [38]. It means that under a higher pumping power, the optimal rectangle microchannel may have superior comprehensive performance to some kinds of enhanced microchannels. And it also demonstrates that it is reasonable to compare the Pareto frontiers of different types of microchannels and select the superior one considering the users' requirements, instead of comparing the structures with specific geometric parameters under some specific conditions to declare which one is superior.

In summary, the above analyses suggest that the comprehensive evaluation method developed in this paper can select the best one from various enhanced microchannel heat sinks through comparing the DOA in Pareto frontiers determined by the limits or priorities of users with high accuracy and immediacy. It is obvious that the hybrid microchannel heat sink combining manifold with secondary channels proposed in our previous work has the largest DOA among those four enhanced structures, which means that under those studied conditions, our hybrid microchannel cooling strategy can maintain a lower thermal resistance under the same pumping power. It should be noted that if researchers or engineers value other evaluation criteria, such as  $h$ ,  $Nu$ ,  $f$ , or  $PEC$ , due to their limits or priorities, they can certainly use those evaluation criteria to evaluate the performance of microchannel heat sinks. However, the comparison should be carried out between the DOAs in Pareto frontiers of those optimal designs.

#### 4. Conclusions

In this work, a comprehensive performance evaluation method based on the Pareto frontier for different types of enhanced microchannel heat sinks is proposed. The immediacy and accuracy of the comprehensive evaluation method are verified through detailed comparisons of DOA for different types of enhanced microchannel heat sinks. The key conclusions are as follows:

- (1) The concept of Design Optimization Area developed in our previous work is used to evaluate the comprehensive performance of different types of microchannel heat sinks. A microchannel heat sink within DOA means that the pumping power and the total thermal resistance could be both reduced compared with user demands. A larger DOA suggests that more microchannel heat sinks of a given type with specific geometric parameters can meet

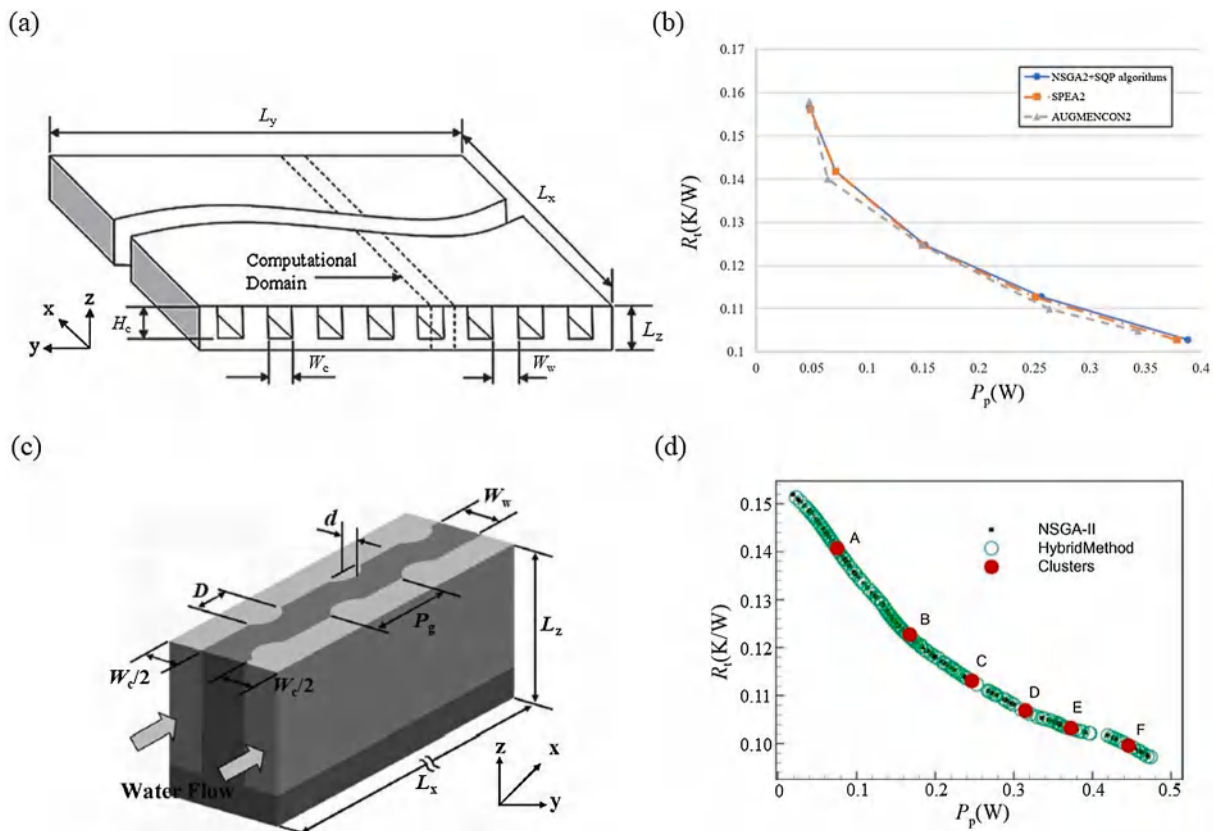


Fig. 20. (a) The microchannel structure and (b) the Pareto frontier of the heat sink selected by Kwanda et al. [38]. (c) The microchannel structure and (d) the Pareto frontier of the heat sink proposed by Ansari et al. [39].

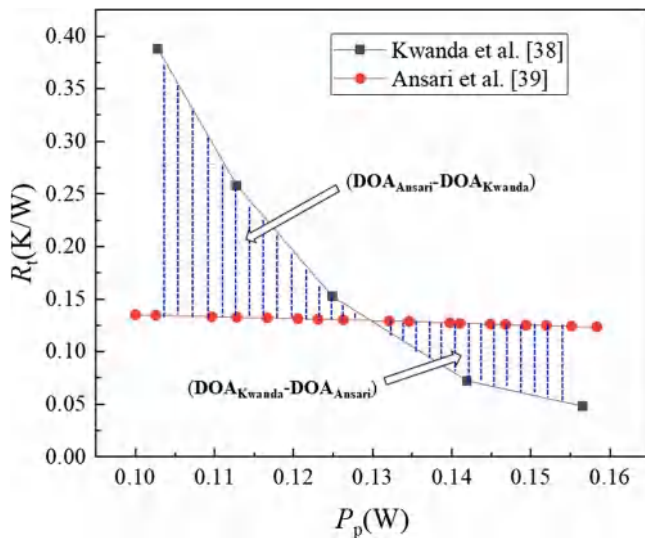


Fig. 21. Comparison of DOA of the microchannel heat sink proposed by Kwanda et al. [38] and Ansari et al. [39].

user demands. The region of DOA can be determined according to the requirements of users;

- (2) The comprehensive evaluation method consists of three steps: 1) conducting a multi-objective thermal and hydraulic design optimization of various microchannel heat sinks to obtain the Pareto frontiers; 2) determining the region of Design Optimization Area above those Pareto frontiers based on the limits or priorities of users or designers; 3) selecting the best one with the largest DOA area. The immediacy and practicability of the method are verified through comparative studies between the Pareto frontiers of two types of heat sinks;
- (3) Careful comparisons have been conducted by selecting different microchannel structures. Furthermore, it shows that the hybrid microchannel heat sink proposed in our previous study has larger DOA by comparing with the other three enhanced microchannel structures, i.e. microchannel with cavity and rib, microchannel with wire coil inserts and interrupted microchannel with rib, based on this method. The results mean that our design enables a lower pumping power under the same total thermal resistance within a certain range;
- (4) This performance evaluation method is helpful for users to find the best one from various types of microchannel heat sinks. Furthermore, by changing the optimization objectives according to the limits or priorities of users, this method could enable the comprehensive evaluation of various heat exchangers, such as refrigeration, air conditioning and energy recovery systems, etc.

#### Declaration of Competing Interest

The authors declare that they have no known competing financial interests or personal relationships that could have appeared to influence the work reported in this paper.

#### Acknowledgement

This project was supported by the National Natural Science Foundation of China (Grant Nos. U20A20301, 51825601).

#### References

- [1] B.T. Li, C.H. Xie, X.X. Yin, R. Lu, Y. Ma, H.L. Liu, J. Hong, Multidisciplinary optimization of liquid cooled heat sinks with compound jet/channel structures arranged in a multipass configuration, *Appl. Therm. Eng.* 195 (2021) 117159, <https://doi.org/10.1016/j.applthermaleng.2021.117159>.
- [2] Y. Alihosseini, M. Zabetian Targhi, M.M. Heyhat, N. Ghorbani, Effect of a micro heat sink geometric design on thermo-hydraulic performance: A review, *Appl. Therm. Eng.* 170 (2020) 114974, <https://doi.org/10.1016/j.applthermaleng.2020.114974>.
- [3] W.M.A.A. Japar, N.A.C. Sidik, R. Saidur, Y. Asako, S. Nurul Akmal Yusof, A review of passive methods in microchannel heat sink application through advanced geometric structure and nanofluids: Current advancements and challenges, *Nanotechnol. Rev.* 9 (2020) 1192–1216, <https://doi.org/10.1515/ntrveng-2020-0094>.
- [4] F. Li, Q. Ma, G. Xin, J. Zhang, X. Wang, Heat transfer and flow characteristics of microchannels with solid and porous ribs, *Appl. Therm. Eng.* 178 (2020) 115639, <https://doi.org/10.1016/j.applthermaleng.2020.115639>.
- [5] C.H. Hoang, S. Rangarajan, S. Khalili, B. Ramakrisnan, V. Radmard, Y. Hadad, S. Schifres, B. Sammakia, Hybrid microchannel/multi-jet two-phase heat sink: A benchmark and geometry optimization study of commercial product, *Int. J. Heat Mass Transf.* 169 (2021) 120920, <https://doi.org/10.1016/j.ijheatmasstransfer.2021.120920>.
- [6] H.-L. Li, D.-Y. Lan, X.-M. Zhang, B.-Y. Cao, Investigation of the Parameter-Dependence of Topology-Optimized Heat Sinks in Natural Convection, *Heat Transfer Eng.* 43 (11) (2022) 922–936, <https://doi.org/10.1080/01457632.2021.1919972>.
- [7] J.-H. Meng, H.-C. Wu, L. Wang, G. Lu, K. Zhang, W.-M. Yan, Thermal management of a flexible controlled thermoelectric energy conversion-utilization system using a multi-objective optimization, *Appl. Therm. Eng.* 179 (2020) 115721, <https://doi.org/10.1016/j.applthermaleng.2020.115721>.
- [8] J.-H. Meng, H.-C. Wu, D.-Y. Gao, Z. Kai, G. Lu, W.-M. Yan, A novel super-cooling enhancement method for a two-stage thermoelectric cooler using integrated triangular-square current pulses, *ENERGY* 217 (2021) 119360, <https://doi.org/10.1016/j.energy.2020.119360>.
- [9] D.B. Tuckerman, R.F.W. Pease, High-performance heat sinking for VLSI, *IEEE Electron Device Lett.* EDL-2 2 (5) (1981) 126–129, <https://doi.org/10.1109/EDL.1981.25367>.
- [10] W. Qu, I. Mudawar, Experimental and numerical study of pressure drop and heat transfer in a single-phase micro-channel heat sink, *Int. J. Heat Mass Transf.* 45 (12) (2002) 2549–2565, [https://doi.org/10.1016/S0017-9310\(01\)00337-4](https://doi.org/10.1016/S0017-9310(01)00337-4).
- [11] H.S. Shamsuddin, P. Estellé, J. Navas, N. Mohd-Ghazali, M. Mohamad, Effects of surfactant and nanofluid on the performance and optimization of a microchannel heat sink, *Int. J. Heat Mass Transf.* 175 (2021) 121336, <https://doi.org/10.1016/j.ijheatmasstransfer.2021.121336>.
- [12] B.o. Sun, H. Wang, Z. Shi, J.i. Li, Pumping power and heating area dependence of thermal resistance for a large-scale microchannel heat sink under extremely high heat flux, *Heat Mass Transfer* 58 (2) (2022) 195–208, <https://doi.org/10.1007/s00231-021-03104-y>.
- [13] L. Chai, L. Wang, X. Bai, Thermohydraulic performance of microchannel heat sinks with triangular ribs on sidewalls – Part 2: Average fluid flow and heat transfer characteristics, *Int. J. Heat Mass Transf.* 128 (2019) 634–648, <https://doi.org/10.1016/j.ijheatmasstransfer.2018.09.027>.
- [14] L.E. Paniagua-Guerra, B. Ramos-Alvarado, Efficient hybrid microjet liquid cooled heat sinks made of photopolymer resin: thermo-fluid characteristics and entropy generation analysis, *Int. J. Heat Mass Transf.* 146 (2020) 118844, <https://doi.org/10.1016/j.ijheatmasstransfer.2019.118844>.
- [15] M. Chen, Y. Wang, Z. Liu, Experimental study on micro-encapsulated phase change material slurry flowing in straight and wavy microchannels, *Appl. Therm. Eng.* 190 (2021) 116841, <https://doi.org/10.1016/j.applthermaleng.2021.116841>.
- [16] S. Singh, S.K. Singh, H.S. Mali, R. Dayal, Numerical investigation of heat transfer in structured rough microchannels subjected to pulsed flow, *Appl. Therm. Eng.* 197 (2021) 117361, <https://doi.org/10.1016/j.applthermaleng.2021.117361>.
- [17] J. Marschewski, R. Brechbühler, S. Jung, P. Ruch, B. Michel, D. Poulikakos, Significant heat transfer enhancement in microchannels with herringbone-inspired microstructures, *Int. J. Heat Mass Transf.* 95 (2016) 755–764, <https://doi.org/10.1016/j.ijheatmasstransfer.2015.12.039>.
- [18] Z. Feng, X. Luo, F. Guo, H. Li, J. Zhang, Numerical investigation on laminar flow and heat transfer in rectangular microchannel heat sink with wire coil inserts, *Appl. Therm. Eng.* 116 (2017) 597–609, <https://doi.org/10.1016/j.applthermaleng.2017.01.091>.
- [19] J. Xu, Y. Song, W. Zhang, H. Zhang, Y. Gan, Numerical simulations of interrupted and conventional microchannel heat sinks, *Int. J. Heat Mass Transf.* 51 (25–26) (2008) 5906–5917, <https://doi.org/10.1016/j.ijheatmasstransfer.2008.05.003>.
- [20] Y.J. Lee, P.S. Lee, S.K. Chou, Enhanced microchannel heat sinks using oblique fins, *ASME 2009 InterPack Conf.* 2 (2009) 253–260, <https://doi.org/10.1115/InterPACK2009-89059>.
- [21] S. Huang, J. Zhao, L. Gong, X. Duan, Thermal performance and structure optimization for slotted microchannel heat sink, *Appl. Therm. Eng.* 115 (2017) 1266–1276, <https://doi.org/10.1016/j.applthermaleng.2016.09.131>.
- [22] Z. Feng, Z. Hu, Y. Lan, Z. Huang, J. Zhang, Effects of geometric parameters of circular pin-fins on fluid flow and heat transfer in an interrupted microchannel heat sink, *Int. J. Therm. Sci.* 165 (2021) 106956, <https://doi.org/10.1016/j.ijthermalsci.2021.106956>.
- [23] W. Gao, J.F. Zhang, Z.G. Qu, W.Q. Tao, Numerical investigations of heat transfer in hybrid microchannel heat sink with multi-jet impinging and trapezoidal fins, *Int. J. Therm. Sci.* 164 (2021) 106902, <https://doi.org/10.1016/j.ijthermalsci.2021.106902>.
- [24] K.P. Drummond, D. Back, M.D. Sinanis, D.B. Janes, D. Peroulis, J.A. Weibel, S. V. Garimella, A hierarchical manifold microchannel heat sink array for high-heat-flux two-phase cooling of electronics, *Int. J. Heat Mass Transf.* 117 (2018) 319–330, <https://doi.org/10.1016/j.ijheatmasstransfer.2017.10.015>.

- [25] W. Li, L. Zhu, F. Ji, J. Yu, Y. Jin, W. Wang, Optimization of Manifold Microchannel Heat Sink inside Interposer, *Electron. Packag. Technol.* 2019 21st Conf. (EPTC 2019). (2019) 66-70. doi: 10.1109/EPTC47984.2019.9026659.
- [26] Y. Luo, J. Zhang, W. Li, A comparative numerical study on two-phase boiling fluid flow and heat transfer in the microchannel heat sink with different manifold arrangements, *Int. J. Heat Mass Transf.* 156 (2020) 119864, <https://doi.org/10.1016/j.ijheatmasstransfer.2020.119864>.
- [27] M. Yang, M.-T. Li, Y.-C. Hua, W. Wang, B.-Y. Cao, Experimental study on single-phase hybrid microchannel cooling using HFE-7100 for liquid-cooled chips, *Int. J. Heat Mass Transf.* 160 (2020) 120230, <https://doi.org/10.1016/j.ijheatmasstransfer.2020.120230>.
- [28] R. van Erp, R. Soleimanzadeh, L. Nela, G. Kampitsis, E. Matioli, Co-designing electronics with microfluidics for more sustainable cooling, *Nature* 585 (7824) (2020) 211–216, <https://doi.org/10.1038/s41586-020-2666-1>.
- [29] K.Y. Lim, Y.M. Hung, B.T. Tan, Performance evaluation of twisted-tape insert induced swirl flow in a laminar thermally developing heat exchanger, *Appl. Therm. Eng.* 121 (2017) 652–661, <https://doi.org/10.1016/j.applthermaleng.2017.04.134>.
- [30] W.T. Ji, J.F. Fan, C.Y. Zhao, W.Q. Tao, A revised performance evaluation method for energy saving effectiveness of heat transfer enhancement techniques, *Int. J. Heat Mass Transf.* 138 (2019) 1142–1153, <https://doi.org/10.1016/j.ijheatmasstransfer.2019.04.128>.
- [31] Y.-L. He, S.-Z. Tang, W.-Q. Tao, M.-J. Li, F.-L. Wang, A general and rapid method for performance evaluation of enhanced heat transfer techniques, *Int. J. Heat Mass Transf.* 145 (2019) 118780, <https://doi.org/10.1016/j.ijheatmasstransfer.2019.118780>.
- [32] P. Yao, Y. Zhai, M. Ma, Y. Li, H. Wang, An improving performance evaluation plot (PEP) for energy management in microchannel heat sinks by using nanofluids, *Int. Commun. Heat Mass* 117 (2020) 104808, <https://doi.org/10.1016/j.icheatmasstransfer.2020.104808>.
- [33] J. Shen, Z. Tu, S.H. Chan, Evaluation criterion of different flow field patterns in a proton exchange membrane fuel cell, *Energ. Convers. Manage.* 213 (2020) 112841, <https://doi.org/10.1016/j.enconman.2020.112841>.
- [34] M. Yang, B.-Y. Cao, Numerical study on flow and heat transfer of a hybrid microchannel cooling scheme using manifold arrangement and secondary channels, *Appl. Therm. Eng.* 159 (2019) 113896, <https://doi.org/10.1016/j.applthermaleng.2019.113896>.
- [35] M. Yang, B.Y. Cao, Multi-objective optimization of a hybrid microchannel heat sink with manifold arrangement and secondary channels, *Appl. Therm. Eng.* 181 (2020), 115592, <https://doi.org/10.1016/j.applthermaleng.2020.115592>.
- [36] Y.L. Zhai, *Flow visualization and thermodynamic analysis of the heat transfer process in micro heat sinks with complex structure*, Beijing University of Technology, Beijing, 2015 in Chinese.
- [37] L. Chai, L. Wang, Thermal-hydraulic performance of interrupted microchannel heat sinks with different rib geometries in transverse microchambers, *Int. J. Therm. Sci.* 127 (2018) 201–212, <https://doi.org/10.1016/j.ijthermalsci.2018.01.029>.
- [38] L. Tartibu Kwanda, Multi-objective optimization of a rectangular micro-channel heat sink using the augmented  $\epsilon$ -constraint method, *Eng Optimiz.* 52 (1) (2020) 22–36, <https://doi.org/10.1080/0305215X.2019.1574346>.
- [39] D. Ansari, A. Husain, K.-Y. Kim, Multiobjective Optimization of a Grooved Micro-Channel Heat Sink, *IEEE Transactions on Components and Packaging Technologies*, 33 (2010) 767-776. *IEEE Transactions on Components and Packaging Technologies*, 10.1109/tcapt.2010.2070874.